Radiation Losses of a Theta Pinch Plasma in the Wavelength Range 100 - 200 Ångstroms

W. Engelhardt

IPP 1/108 June 1971

MAX-PLANCK-INSTITUT FÜR PLASMAPHYSIK

GARCHING BEI MÜNCHEN

MAX-PLANCK-INSTITUT FÜR PLASMAPHYSIK

GARCHING BEI MÜNCHEN

Radiation Losses of a Theta Pinch Plasma in the Wavelength Range 100 - 200 Ångstroms

W. Engelhardt

IPP 1/108 June 1971

Die nachstehende Arbeit wurde im Rahmen des Vertrages zwischen dem Max-Planck-Institut für Plasmaphysik und der Europäischen Atomgemeinschaft über die Zusammenarbeit auf dem Gebiete der Plasmaphysik durchgeführt.

IPP 1/108

Wolfgang Engelhardt

Radiation Losses of a Theta Pinch Plasma in the Wavelength Range 10 - 200 Ångstroms.

June 1971 (in English)

Abstract

In order to measure the radiation losses of a theta pinch plasma (electron density $n_e = 1 - 5 \times 10^{16} cm^{-3}$, electron temperature $T_e = 150 - 350$ eV), a grazing incidence spectrograph is absolutely calibrated in the range 10 - 200 Å. This is done in two steps: First the measured intensity ratios of lines emitted by hydrogen-like ions are compared with their calculated values thus yielding the relative sensitivity of the instrument. The result is confirmed by incorporating well known intensity ratios of lithium-like ions. Secondly absolute calibration is possible by hanging the spectrograph on an absolutely calibrated monochromator via the branching-ratios of lithium-like ions.

Radiation losses from the plasma turn out to be negligible as compared with heat conduction losses and the whole energy radiated is found to be small compared with the energy content of the electrons, if the impurity concentration does not exceed 0.5 percent. The radiation is found to be predominantly emitted by the resonance lines of the oxygen and carbon ions O VI, O VII, O VIII, C, V, C VI whereas continuum radiation and the contribution from other ions are negligible small.

However in discharges where the oxygen concentration reaches 5 percent, radiation losses can exceed the losses by heat conduction during the early phase of the discharge. But still the final electron temperature is not significantly influenced by the impurities.

Index

1. Introduction

The production of a plasma in a theta pinch is characterized by two phases: 1. Fast compression that is completed in a few 100 nsec and raises the energy of mainly the ions by shock heating; 2. subsequent slow, adiabatic compression that raises the energy of the ions and electrons in the same way. In both phases the electrons also gain energy by ohmic heating. At the end of the first phase the ions have a higher temperature than the electrons; this difference should disappear after a sufficient long time as a result of relaxation. Numerous measurements /e.g.1/ now show that such energy equipartition is usually not achieved, rather does the electron temperature remain below the ion temperature. There are apparently loss mechanisms that cool the electrons more strongly than the ions. Two explanations have been suggested:

1. Energy loss due to both continuum and line radiation /2/,
2. Loss of electron energy due to thermal conduction to the vessel wall, provided that the plasma touches it at a few points at least /1/.

This report is concerned with the first mechanism, the main purpose being to investigate the line radiation quantitatively. While the free-free or recombination continuum radiation can be fairly reliably calculated if the electron temperature and density and the chemical composition of the plasma are known, this is not possible with the line radiation for various reasons. One would have to know the concentration of the ionization stages of the impurity atoms, the populations of the excitation levels, and finally the corresponding transition probabilities. The latter are the most likely to be known; For calculating the populations it is frequently necessary, viz. when the plasma is not in thermal equilibrium, to know the excitation and ionization cross sections in addition to the plasma parameters. This applies particularly to the levels of the high-energy resonance transitions, which are very seldom thermally populated. Knowledge of the cross sections and hence of the rate coefficients is still very sketchy. Only with ions of very simple structure such as hydrogen-like or lithium-like ions can they be estimated,

and this only allows the radiation losses to be predicted to within one order of magnitude /2 - 5/. It is therefore attempted here to determine experimentally the energy losses due to line radiation.

The spectral range in which the bulk of the radiation will occur can be roughly defined by simplification: The electron temperature in a theta pinch reaches a few 100 eV. Impurities therefore mainly occur in ionization stages requiring energies of between 100 and 1000 eV for further ionization. For the principal impurities: carbon, nitrogen, oxygen, and silicon, this means the stages C V-VI, N VI-VII, O VI-VIII, Si V-XII. The most energetic transitions /6/ of these ions are mainly in the range 10 - 200 Å. At an electron temperature of between 100 and 500 eV the maximum of the free-free continuum radiation also occurs in this region. The investigations were therefore only conducted within the given limits.

The radiation is spectrally resolved with a grazing incidence spectrograph and recorded with photographic plates and scintillator-SEM assemblies. Absolute calibration of the spectrograph presents problems since there is no radiation standard in the spectral region investigated[1)]. One therefore has to hang the spectrograph on a radiation standard in the visible range, this being possible by the branching ratio method /7/. This only allows calibration at very few points of the spectrum, and so relative calibration covering the whole spectrum if possible has to be attempted as well.

The first part of the report briefly describes the experimental set-up. The major part following deals with the calibration method, while the remaining part gives the results of the radiation measurements.

---

1) Using an electron synchrotron was rejected for technical reasons.

2. Experimental set-up and plasma parameters

The measurements were made on a linear theta pinch (ISAR II). The technical details of this device are given in /8/. Only the most important data on which the experiment was based are listed here:

Charging voltage	25 kV
Stored energy	195 kJ
Maximum magnetic field	51.5 kG
Magnetic field rise	28.9 kG/µsec
Quarter-cycle	2.8 µsec
Crowbar time constant	50 µsec
Antiparallel bias field	0 - 500 G
Filling pressure	10 - 80 mTorr deuterium
Coil length	100 cm
Coil diameter	10.7 cm
Vessel diameter (inner)	9 cm

The coil is divided in two sections to allow symmetric current feed and double the applied voltage relative to the charging voltage. This results in a fast magnetic field rise and hence effective shock heating in the initial phase.

The plasma parameters were measured by Köppendörfer et al. /9/, the electron density being determined by three independent methods: 1. absolute measurement of the continuum radiation in the visible range, 2. absolute measurement of scattered laser light, 3. interferometric measurement of the refractive index of the plasma. The electron temperature was determined both from the laser scattering measurement and by the X-ray absorption method. Lastly, the ion temperature was found from the measured neutron yield. Details are given in /9/. Only the results of the laser scattering measurement are shown in Fig.1, since they allow the most accurate temperature determination and also because knowing the electron temperature was important for calibrating the spectrograph, as will become apparent later.

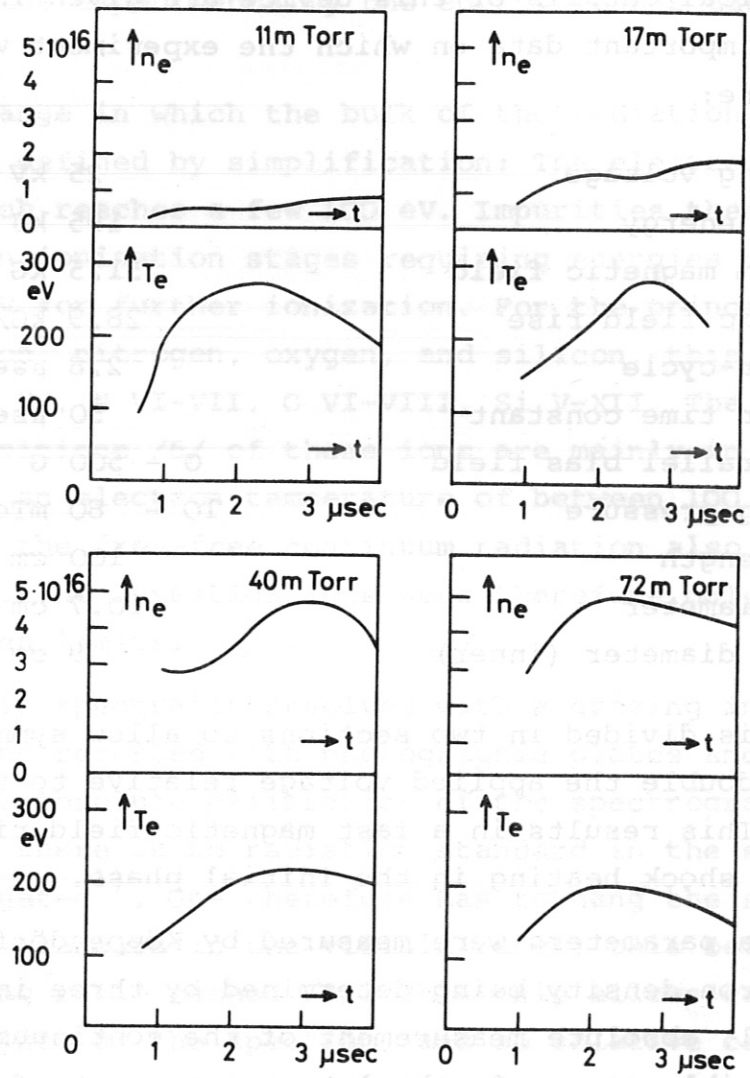

Fig. 1 Electron temperature and density as functions of time (measurement by Thomson scattering of laser light in the mid-plane of the coil on the axis).

3. Calibration of the spectrograph

3.1 Technical data of the spectrograph

The spectrograph used was a McPherson Model 246, which is suitable both for recording time integrated spectra on photographic plates and for time resolved photoelectric recording of radiation. It was screwed end-on to the discharge tube at a distance of about 2m from the coil centre. The vessel was filled about 1 sec before the discharge, and so only a small amount of deuterium had time to flow into the spectrograph through the narrow entrance slit: The pressure rise at the time of the discharge was smaller than 10^{-5} torr. The technical data of the instrument are listed in the table below, only the settings actually used in the experiment being included.

Spectrograph:

Diameter of the Rowland circle	221.7 cm
Angle of incidence	86.5 ^{o}
Aperture ratio	$\approx$ 1 : 100
Entrance slit width	0.010 mm
Exit slit width (in multiplier operation)	0.025 mm

Grating:

Manufacturer	Bausch & Lomb
Material	Gold
Ruling	600 lines per mm
Blaze angle	1.5^{o}

Detector:

1. Ilford Q 2 plates	2" x 10" x 0.04"
2. Scintillators	$\lambda < 40$ Å plastic scintillator NE 102 A coated with aluminium
	$\lambda > 40$ Å liumogen /10/
Multiplier	RCA 1 P 28 in all cases

The fluorescent light is directly recorded, i.e. without use of a light pipe.

The resolution for the given entrance slit width is governed by purely geometrical considerations /11/. The apparatus profile should be rectangular in shape and have the width $\Delta\lambda = d \cdot b/R$ irrespective of the wavelength (d= grating constant, R = diameter of the Rowlandcircle, b = entrance slit width). Substituting the values from the table provided yields $\Delta\lambda = 0.075$ Å. For $\lambda = 100$ Å the resolution is therefore $\Delta\lambda/\lambda = 7.5 \times 10^{-4}$ Å. This value was in fact obtained with careful adjustment.

3.2 Principle of the calibration method

The instrument is calibrated together with the photographic plate. If a certain energy E passes through the entrance slit at a wavelength λ, part of the energy E' is reflected by the grating and impinges on the plate. The resulting density is then

$$D = \gamma \log \frac{E'}{E_o} = \gamma \log \frac{s' E}{E_o} = \gamma \log (sE) \qquad (1)$$

D = density, γ = slope of the density curve in the linear part, E_o = speed of the plate, s' = permeability of the instrument.

All these quantities are functions of λ. The above relation is only valid, of course, in the linear part of the density curve. Calibration constists in determining the quantities $\gamma(\lambda)$ and $s(\lambda)$.

The value γ can be obtained in a relatively simple manner: One can record the line spectrum of the plasma being investigated placing meshes of known geometric permeability at a suitable point in the beam path. This provides defined reduction of the energy input and the differences in density measured with a microdensitometer give the density curve or γ as a function of the wavelength. This is conditional upon the light source, in this case the plasma, radiating with reproducible intensity over the whole wavelength range. This was achieved by strictly ensuring equal initial conditions for the discharge (charging voltage, filling pressure, impurity concentration). Four spectra of different densities could be recorded together on one plate, and so four points of the density curve

were obtained for every sufficiently intense line. Each set of four points fixed the straight line with the least square error, its slope representing the γ of the respective wavelength. The function $\gamma(\lambda)$ thus measured is plotted in Fig.2. The plates were always developed (with Kodak developer D 19 b) under the same conditions, and so the γ = values for various plates only differ slightly. It was therefore not necessary to determine the density curve again for each plate in the actual radiation measurements. The measuring error for γ is about 20 %; it is determined from different results for closely spaced lines.

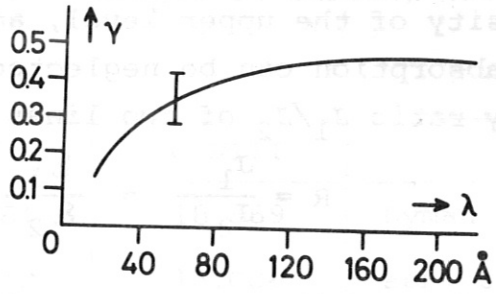

Fig.2 Slope of the density curve for Ilford Q 2 emulsion as a function of the wavelength.

Measuring the quantity s in eq.(1), which allows for both the permeability of the instrument and the speed of the plate, is a much more difficult proposition. This calls for a light source of known spectral intensity distribution. Such a light source is afforded by, for example, the continuum of an X-ray tube, whose intensity distribution could be measured with a proportional counter, but not very accurately, or the continuum of a suitable plasma whose composition and state variables are known with sufficient exactness. Both cases involve only low intensities thus making long exposure times necessary. Furthermore it is difficult to discriminate against scattered radiation from intense lines that are superposed on the continuum.

If continous calibration in the whole spectral range is dispensed with and only individual spectral lines of known intensity ratio are used, these disadvantages can be avoided. Calibration is then obtained at individual points of the spectrum, between which one has to interpolate. This approach was adopted here since enough suitable line pairs were found and it could be assumed that the calibration curve is smooth between the lines. The emission coefficient ε of a spectral line is given by:

$$\varepsilon = \frac{h\nu}{4\pi} n A \qquad (2)$$

where $h\nu$ is the energy of the emitted quantum, n the population density of the upper level, and A the transition probability. If absorption can be neglected (optically thin case), the intensity ratio J_1/J_2 of two lines is

$$R = \frac{J_1}{J_2} = \frac{\varepsilon_1}{\varepsilon_2} = \frac{\lambda_2 n_1 A_1}{\lambda_1 n_2 A_2} . \qquad (3)$$

If the two lines originate from the same ion, it can also be assumed that

$$\frac{\int J_1 \, dt}{\int J_2 \, dt} = R = \frac{E_1}{E_2} . \qquad (4)$$

With equation (1) this gives

$$\frac{s(\lambda_1)}{s(\lambda_2)} = \frac{1}{R} \cdot 10^{(D_1/\gamma_1 - D_2/\gamma_2)} \qquad (5)$$

The function $s(\lambda)$ can thus be determined relatively if the intensity ratios of a sufficiently large number of line pairs are known. This relative calibration can then be made absolutely if the intensity of at least one line is measured absolutely.

In order to determine R (eq. (3)), the ratio of the populations n_1/n_2 is also required in addition to the wavelengths and transition probabilities, which are frequently known. Calculating this ratio turns out to be the real problem because the populations in the non-equilibrium plasma investigated cannot be handled simply by using Boltzmann factors. In some cases it was possible to calculate

the population ratio, in others the branching ratio method /7/ could be used because the lines originated from the same level and hence the population ratio was exactly 1. The next section deals in detail with the line ratios used.

3.3 Intensity ratios of lines in the grazing incidence region

3.3.1 Line ratios in the Lyman and Balmer series of hydrogen-like ions

Line ratios can be readily calculated by using hydrogen-like ions because owing to their simple structure the transition probabilities are well known /12/ and the excitation coefficients /13/ fairly well known. Table 1 lists the wavelengths /14/ of the transitions observed in the hydrogen-like ionization stages of carbon, nitrogen, and oxygen.

Transition q-q'	C VI	N V	O VIII	
1 - 2	33.736	24.781	18.969	Lyman
1 - 3	28.466	20.910	16.006	series
1 - 4	26.990	19.826	15.176	
2 - 3	182.16	133.82	102.43	
2 - 4	134.95	99.13	75.89	Balmer
2 - 5	120.50	88.51	67.76	series

Table 1 Wavelengths of hydrogen-like ions (in Å units)

It is readily seen that the wavelengths of the transition CVI 2 - 4 almost coincides with that of the transition NVII 2 - 3. The same holds for the tranitions NVII 2 - 4 and OVIII 2 - 3. Thus, if the ratio of the first Balmer lines 2 - 3/2 - 4 is known for all these ions, the spectral range 76 - 182 Å can be covered more or less completely. Line ratios in the Balmer series will therefore be calculated first; the same reasoning can then be extended to the Lyman series.

According to Griem /15/ the collision limit for CVI with the given plasma parameters $n_e = 1 - 4 \times 10^{16} cm^{-3}$ and $kT_e = 200 - 300$ eV is at the effective quantum number $q_{eff} = 5.8$. That is, above the level q = 6 the population is approximately thermal, while below q = 5 it is governed by corona equilibrium. According to Table 1 the levels of the Balmer series are below $q_{eff} = 5.8$. Corona equilibrium /7/ can therefore be used to calculate their population ratios. If only excitation from the ground state is considered, it holds approximately for the first two Balmer lines[1]:

$$n_e n_1 X_{13} \approx n_3 \cdot \sum_{q<3} A_{3q} - n_4 A_{43} \qquad (6a)$$

$$n_e n_1 X_{14} \approx n_4 \cdot \sum_{q<4} A_{4q} \qquad (6b)$$

Dividing then gives:

$$\frac{n_3}{n_4} = \frac{X_{13}}{X_{14}} \frac{\sum A_{4q}}{\sum A_{3q}} + \frac{A_{43}}{\sum A_{3q}} \qquad (6)$$

where n_q is the population of the principal quantum number q, $A_{qq'}$, the transition probability between q and q', X_{1q} the excitation coefficient from the ground state to the principal quantum state q. With a Maxwell distribution of the electrons, it holds for the excitation coefficients according to Allen /13/:

$$X_{1q} \propto \frac{f_{1q}}{(kT_e)^{1/2} E_{1q}} \exp(-E_{1q}/kT_e) \cdot P(E_{1q}/kT_e) \qquad (7)$$

where f_{1q} is the absorption oscillator strength of the corresponding allowed optical transition, E_{1q} the excitation energy, and kT_e the electron temperature. $P(E_{1q}/kT_e)$ is a function varying weakly with E_{1q}/kT_e. The ratio of the two excitation coefficients is then

$$\frac{X_{13}}{X_{14}} \approx \frac{f_{13}}{f_{14}} \frac{\lambda_{31}}{\lambda_{41}} \exp(E_{34}/kT_e) \cdot 1 \qquad (8)$$

---

[1] The approximations are discussed at the end of this section.

This ratio depends only slightly on the temperature since $E_{34} \approx 30$ eV $\ll kT_e$, and so it is sufficient to insert an approximate temperature. It is now possible to calculate the required intensity ratio of the first two Balmer lines from eqs. (8), (6), and (3):

$$\frac{J_{32}}{J_{42}} = \frac{\lambda_{42} A_{32}}{\lambda_{32} A_{42}} \left[\frac{f_{13}}{f_{14}} \frac{\lambda_{31}}{\lambda_{41}} \exp(E_{34}/kT_e) \frac{\sum A_{4q}}{\sum A_{3q}} + \frac{A_{43}}{A_{3q}} \right] \quad (9)$$

The calculation for the ratio of the transitions 4 - 2 / 5 - 2 is completely analogous. It should be noted, however, that the level q = 5 for CVI at least is already very close to the collision limit and may be depopulated into the continuum by electron collisions. So the intensity ratio of the higher transitions calculated under the assumption of corona equilibrium should only be regarded as correct for OVIII and NVII; deviations may already occur for CVI.

The same applies in the Lyman series. Eq. (9) in appropriately modified form allows the ratios 1 - 2 / 1 - 3 / 1 - 4 to be calculated for each ion. However, the wavelengths of individual transitions for various ions do not coincide in the same way (see Table 1) as in the Balmer series. The ratios for various ions thus do not directly adjoin one another, and the shortwave part of the spectrum cannot be completely covered. It was therefore attempted to join this region directly to the long-wave part of the spectrum by means of branching ratios and use the line ratios in the Lyman series for intermediate points only. The branching ratios are discussed in a later section; first a few critical remarks will be made on the line ratios calculated above.

We have tacitly proceeded from a number of assumptions:

1) Sub-levels with the same principal quantum number but different orbital angular momentum quantum number are populated according to their statistical weight.
2) The ratio of the excitation coefficients $X_{1q} / X_{1(q+1)}$ can be set equal to that of those excitation coefficients for which there are corresponding optically allowed transitions. That is excitation transitions from the ground state to the qP level are representative of all other collisional transitions.

3) The population of all higher levels by collisions starts from the ground state only.
4) Radiation transitions from levels $q' > 4$ do not contribute to the population of level $q = 4$.

Assumption 1) is certainly not sufficiently satisfied. Statistical population would be present if sufficient collisions take place in the sublevels before transition to a lower principal quantum number occurs. According to Allen /13/ and Wiese et al./12/ an excitation rate of $n_e X_{33} \approx 10^7$ sec^{-1} (kT_e = 200 eV, $n_e = 4 \times 10^{16}$ cm^{-3}) is obtained for the fine structure transition $3\,^2S_{1/2} - 3\,^2P_{3/2}$ for NVII. This value has to be compared with the transition probability $A_{3P1S} = 4 \times 10^{11}$ sec^{-1}. There are thus much more radiative transitions to the ground state per unit time than collisional transitions in the sublevels, which means that the sublevels need not be statistically populated by any means. Strictly speaking, it is consequently not legitimate to take corona equilibrium for the whole set of levels with the same principal quantum number; instead this has to be done separately for each sub-series with the same orbital angular momentum. The calculation then contains all excitation coefficients, including those for collisional transitions without corresponding radiative dipole transitions. As very few excitation cross sections are known for hydrogen-like ions /16/, this procedure cannot readily be carried out. In order to get at least an idea of the order of magnitude by which a detailed calculation deviates from the overall result (eq.(9)), the intensities of the Balmer lines were calculated again on the basis of excitation cross sections of atomic hydrogen /17/ completely neglecting collisions between sublevels. It was found that the results differ only about 15 % from the previous values although devations of up to a factor of 20 from statistical population occured. The small difference is mainly due to the fact that assumtion 2) proved to be well satisfied. The calculation showed that in this case deviations from statistical population only slightly affect the intensity ratio. This, of course, applies only to atomic hydrogen. But it should not be very much different for ions because it is always only the ratios of excitation coefficients that are used, not absolute values.

The deviation from statistical population is in fact certainly smaller than that resulting when collisions in the sub-levels are completely neglected. There are experimental grounds to support this: Firstly, the intensity ratio of the fine structure components of the Balmer lines can be calculated from the population of the sub-levels. Secondly, this ratio can also be measured. It is then found that the experimental value deviates 30 % from the calculated one. This means that the real population is closer to the statistical value than the simplified calculation predicts. The difference of 15 % between the detailed and the overall calculation is thus further reduced. Only the simple result (eq. (9)) was therefore used for calibration.

Assumption 3) is probably well satisfied because for all levels there are large transition probabilities to all lower levels, and so their population is small relative to the ground state. One exception is the metastable level 2S, which can only be depopulated by collisions[1]. Electron collisions induce transitions to 2P and 3P with a ratio of about 2 : 3. Ion collisions, however, shift the ratio in favour of the 2P level owing to the small energy difference between 2S and 2P. For this reason the additional population derived by level 3 from the metastable level 2S is of hardly any significance, and so the intensity ratios are not affected much.

The correctness of assumption 4) is relatively easy to check. In eq. (6a) the term $n_4 A_{43}$, which allows for the radiative transition from $q = 4$, proved to be small compared with the collision term $n_e n_1 X_{13}$, This must be all the more true of the neglected terms $n_q A_{q3}$ $(q > 4)$. Furthermore, radiation transitions from these levels contribute to the additional population of <u>all</u> lower levels, and so the error incurred in forming the ratio of the populations is partly cancelled.

3.3.2 <u>Branching ratios of hydrogen-like ions</u>

This section is concerned with the calculation of line ratios in which one line belongs to the Balmer series and the second to the Lyman series. When the initial levels have the same principal

---

[1] Two photon recombination can be neglected owing to the low transition probability relative to the collision rates.

quantum number, the line ratio in this case should be given simply by /7/:

$$\frac{J_{q2}}{J_{q1}} = \frac{\lambda_{q1}\, A_{q2}}{\lambda_{q2}\, A_{q1}} \qquad (10)$$

Equation (10) is only valid when the sub-levels are statistically populated. As was shown in the previous section, however, this is not the case. It will be found that the population actually present could not be given in detail. It was possible, however, to obtain appropriately corrected branching ratios from the measurement of the intensity ratio of the fine structure components of the first Balmer lines.

The transition 2 - 3 is composed of seven individual transitions, which can be divided into two groups according to their wavelengths (fig.3): The transitions ending in the level $2S_{1/2}$ or $2P_{1/2}$ constitute the short-wave component, while the remaining transitions to the level $2P_{3/2}$ form the long-wave component. The separation between the two components is about 0.15 Å irrespective of the ion

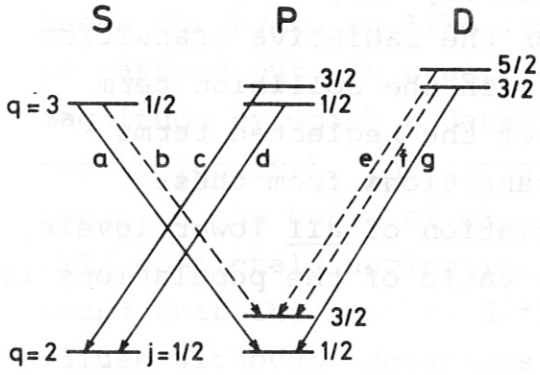

Fig.3a Term scheme of the first Balmer transition of hydrogen

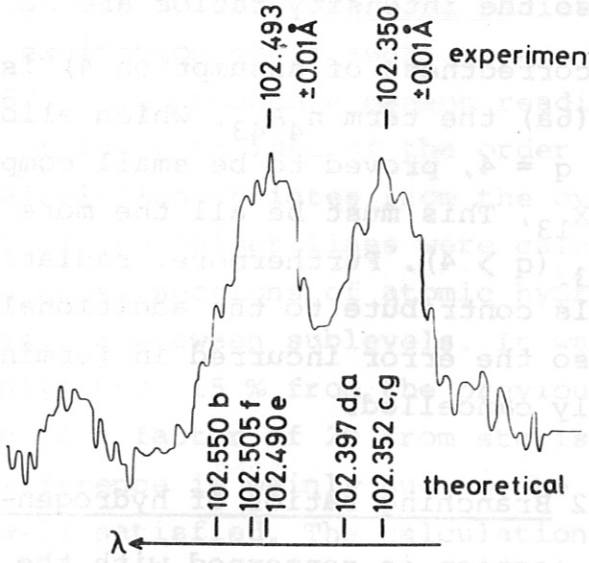

Fig.3b Densitometer curve of the first Balmer doublet for OVIII. (The letters a - g are used to denote the same transitions in Figs.3a - 3b).

and is thus resolvable by the spectrograph. The fine structure within a component can, however, no longer be resolved. The branching ratio according to eq. (10) only holds exactly for the ratio of the transitions 2S - 3P /1S - 3P. Since $2P_{1/2}$ - $3D_{3/2}$ and $2P_{1/2}$ - $3S_{1/2}$ are superposed on 2S - 3P, the populations of the levels $3D_{3/2}$ have to be known in order to subtract the intensity of the disturbing lines. It is, however, already sufficient to know the ratios n_{3P}/n_{3S} and n_{3D}/n_{3P} because it can be assumed that the sub-levels with the same orbital angular momentum quantum number, but different spin orientation are statistically populated. This assumption follows from two facts:

1) Seaton and Percival /18/ show that the excitation cross sections for sub-levels of different spin orientation ($j_1 = 1/2$, $j_2 = 3/2$) are proportional to the statistical weight $2j + 1$, and so the sublevels are statistically populated in the event of collisional excitation from the ground state, 2) depopulation is only due to radiation (corona equilibrium), the transition probabilities /12/ having just the values that cause no change to the statistical population.

The ratios $n_{3D}/n_{3P} \equiv \alpha$ and $n_{3P}/n_{3S} \equiv \beta$ thus determine the intensity ratio (v) of the short-wave to the long-wave component:

$$v = \frac{3\beta A_{3P2S} + A_{3S2P} + \alpha\beta\, A_{3D2P}}{2\,(A_{3S2P} + \alpha\beta\, A_{3D2P})} \qquad (11)$$

For the intensity ratio of the composed individual transitions 2 - 3 / 1 - 3, on the other hand, the following expression is obtained:

$$\frac{J_{32}}{J_{31}} = \frac{\lambda_{31}}{\lambda_{32}} \cdot \frac{A_{3S2P} + \beta A_{3P2S} + \alpha\beta\, A_{3D2P}}{\beta A_{3P1S}} \qquad (12)$$

It is now seen that when eqs. (11) and (12) are combined α and β cancel and only the quantity v apprears in the intensity ratio:

$$\frac{J_{32}}{J_{31}} = R = \frac{\lambda_{31}}{\lambda_{32}} \frac{A_{3P2S}}{A_{3P1S}} \frac{v + 1}{v - 1/2} \quad (13)$$

It thus suffices to determine the ratio v of the fine structure components in order to give the corrected branching ratio R. It is possible to measure v since the two lines are close together and no change in the sensitivity of the spectrograph is expected in such small ranges. It is found that v is different for different ions and depends slightly on the discharge conditions. Furthermore v does not correspond to the statistical value obtained when $\alpha = 5/3$ and $\beta = 3$ are substituted in eq. (11). But even if v did correspond to this value, one is still not entitled to deduce a statistical population for α and β could deviate from the statistical value just enough so that v is preserved. If the Intensity ratio (13) with measured v values is used for calibration, the same calibration points are always obtained for s (λ) under different discharge conditions and for correspondingly different v. This is not the case when the simplified relation (10) is used.

Unfortunately, the method is not too exact. The relative error $\Delta R/R$ can be determined from eq. (13) as a function of v and $\Delta v/v$:

$$\frac{\Delta R}{R} = \frac{3v}{(v-1)(2v-1)} \frac{\Delta v}{v} \quad (14)$$

The slope of the density curve can be determined exactly to within 20 %, and hence v can be measured exactly to within about 7 %. A typical value of v = 0.7 for CVI thus yields

$$\frac{\Delta R}{R} = 3.1 \frac{\Delta v}{v} \approx 0.2 \quad (14a)$$

This means that slight inaccuracies in the measurement of v have an appreciable effect on the exactness of the branching ratio. It can be seen on the other hand, that a small change of v due to a deviation of the population from the statistical value can appreciably change the branching ratio. For example, overpopulation of the 3D level by a factor of 2 relative to the statistical value causes a change of almost 80 % in the branching ratio, while the ratio of the fine structure components varies less than 20 %.

The above reasoning can also be applied in principle to the branching ratios of the transitions 2 - 4 / 1 - 4. In this case, however, the fine structure components of the Balmer lines come so close together that they can no longer be resolved by the spectrograph. It is thus no longer possible to measure v and consequently the branching ratio cannot be given either.

3.3.3 Line ratios of lithium-like ions

The line ratios discussed hitherto suffice in themselves to do the relative calibration. Since, however, there was some uncertainty about the correctness of the relation (9) when applied to the Balmer series, it was attempted to find additional line ratios in the long-wave region that can be calculated. This was only partly successful because it was again necessary to make assumptions that could not be checked exactly. Since, on the other hand, the results confirmed the calibration curve s (λ) already obtained with the hydrogen-like line ratios, it is reasonably certain that not only the theoretical arguments but also the underlying assumptions were correct in both cases.

The lithium-like ions NV and OVI have a large number of transitions in the spectral region between 1oo and 2oo Å. Like the hydrogen-like ions, they are distinguished by particular simplicity. Their transition probabilities are partly calculated /12/, while the rest can be extrapolated from known values /19, 2o/. The transitions concerned are listed in Table 2. The extrapolated transition probabilities are marked with a ?, the other values being taken from /12/.

Transition	O VI		N V	
	λ (Å)	A(10^8 sec^{-1})	λ (Å)	A(10^8 sec^{-1})
2 S - 3 P	150.1	259		
2 P - 3 D	173.0	884		
2 P - 3 S	184.0	170		
2 S - 4 P	115.8	?116	162.6	56.3
2 P - 4 D	129.8	285	186.1	140
2 P - 4 S	132.6	? 62.6	190.2	?35.9
2 S - 5 P	104.8	? 57.7	147.4	?28.1
2 P - 5 D	116.4	?132	166.9	?64.5
2 P - 5 S	117.4	? 31.9		

Table 2 Wavelengths and transition probabilities of lithium -like ions

As in section 3.3.1, it is reasonable to assume corona equilibrium and calculate the population within a series with the same orbital angular momentum. This is hampered, however, by the fact that excitation occurs not only from the ground state 2S, but also from 2P /21/, the population of 2P relative to the ground state being unknown. Furthermore, the necessary cross sections are not available. Use was therefore made of line pairs orginating from the same principal quantum state, but from sub-levels with different orbital angular momentum. Owing to their small energy difference relative to the electron temperature these sub-levels should be populated according to their statistical weights if sufficient collisions take place in the sub-levels. The intensity ratio of the transitions 2S - 3P / 2P - 3D, for example, should be

$$\frac{J_{3P2S}}{J_{3D2P}} = \frac{\lambda_{3D2P}}{\lambda_{3P2S}} \frac{A_{3P2S}}{A_{3D2P}} \frac{n_{3P}}{n_{3D}} \qquad (15)$$

with

$$\frac{n_{3P}}{n_{3D}} \quad \frac{g_{3P}}{g_{3D}} \quad \frac{3}{5} \qquad g = \text{statistical weight} \qquad (16)$$

Actually, electron collisions do not suffice here either to induce such a statistical population (16) because the electron collision rates /13/ are about an order of magnitude smaller than the transition probabilities. Since, however, the deviations were already not so large in the case of hydrogen-like ions as those calculated when collisions in the sub-levels are neglected (section 3.3.1), this will be all the more true of lithium-like ions because for OVI the interval between the level q = 3 and the ionization limit is only 55 eV compared with 96 eV for OVIII. Collisional transitions thus become more probable. The calibration curve already obtained is in fact confirmed in good agreement if one uses all line pairs in Table 2 that originate from P and D levels with the same principal quantum number (see Fig.4). It is therefore reasonable certain that not only is the calibration curve correct, but also the assumption of statistical population for P and D levels of the lithium-like ions. If lines originating from S and P levels are compared, a considerable overpopulation of the S levels is found within the context of our presumably correct calibration curve. There are various explanations for these findings: Overpopulation may only be mistaken because wrong transition probabilities have been used. This, however, would mean that the transition probabilities given by Wiese et al./12/ deviate in this case by a factor of up to 3 from the true value, this being well beyond the error margins assumed in /12/. Another explanation therefore seems more likely: The cross section for collisions between qS - qP sub-levels is particularly small. According to Bely /22/ this is the case for 2S - 3P collisions compared with 2P - 3D transitions. This is presumably true of collisions with no change of the principal quantum number. This, of course, still does not explain why the collision rate is so high as to result in statistical population of P and D levels. It could be that from the outset these levels are populated from the ground state according to their statistical weight, and their population therefore does not have to be equilibrated; possibly, however, ion collisions may contribute to the collision rate. Since the ion temperature is of the order 1 - 2 keV, the ions reach a velocity equivalent to that of electrons with a temperature of about 1 eV. They then presumably collide with the same frequency as

electrons with the temperature 1 eV, thus contributing to the increase of the collision rate. This question, however, goes beyond the scope of this report.

3.3.4 Relative calibration curve

The calibration curve plotted from the discussed line ratios is shown in Fig.4. For clarity the way in which it was obtained is again sketched: The line ratios in the Balmer series allowed the range between 76 and 182 Å to be covered. The transition 2 - 5 of CVI gives a wrong value, presumable because the level q = 5 is already too near the collision limit. The short-wave part of the spectrum was fixed at three points by branching ratios (denoted by arrows in Fig.4); it was confirmed and completed by line ratios in the Lsman series. Confirmation in the long-wave region is provided by the S - P and P - D transitions of the lithium-like ions NV and OVI. The apparently overpopulated S levels yield useless calibration points; the deviations are so large that making allowance for them would give a completely unreasonable calibration curve.

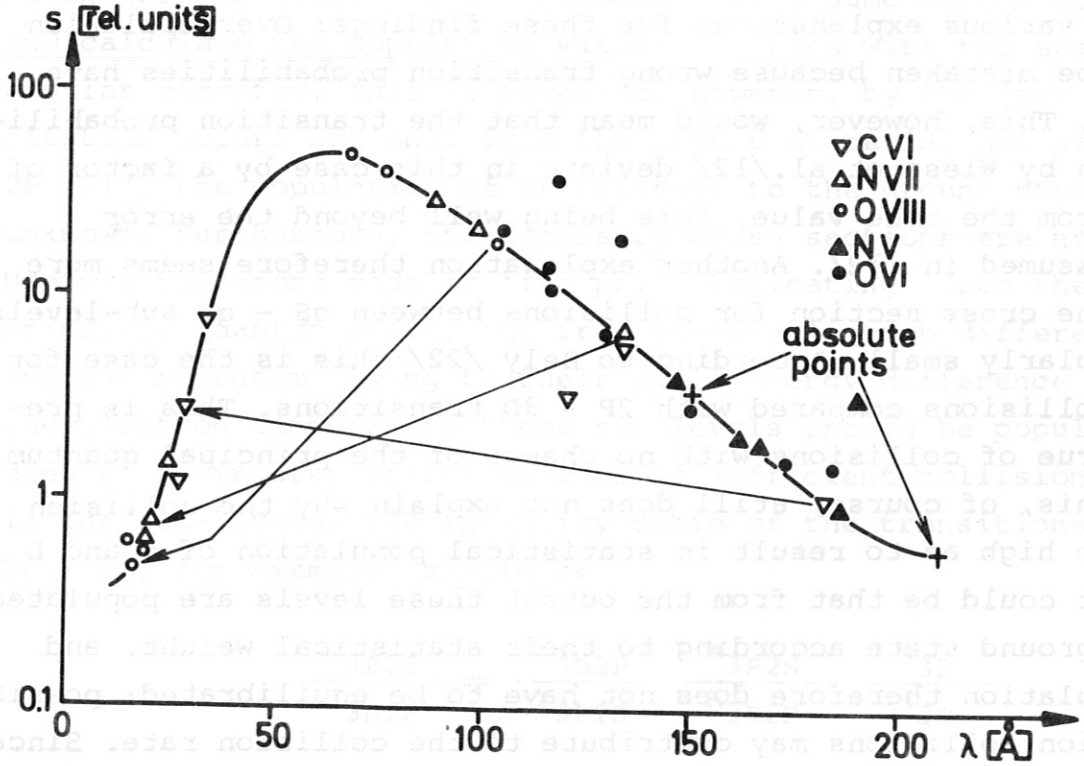

Fig.4: Spectrograph sensitivity as a function of wave length.

Viewed in purely qualitative terms, the result agrees with the predicted curve. At the given angle of incidence the maximum intensity should be reflected into the region of about 50 Å. The reflecting layer is made of gold, for which Lukirskii et al. /23/ give the reflectivity shown in Fig.5 for an angle of incidence of 5° (this being the sum of the grazing and blaze angles in the present case). Because of this behaviour of the reflectivity the maximum should be shifted to longer wavelengths and the drop of the calibration curve ought to be steeper towards short wavelengths than to long wavelengths.

This dependence on λ is borne out by the measured calibration curve; it can thus be concluded that the plate sensitivity E_o, which does in fact appear in the function s (1), varies very little with the wavelength.

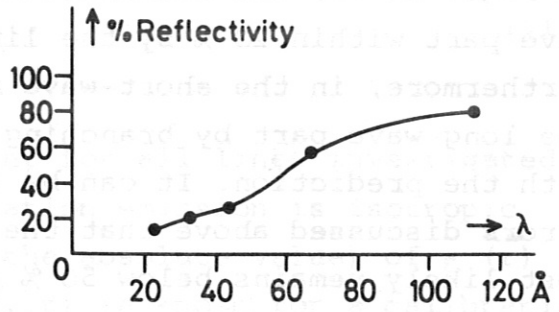

Fig.5 Reflectivity of gold at an angle of incidence of 5°

The accuracy of the calibration curve cannot readily be stated. Both the calculated line ratios R and the measured density differences as well as the measured slope of the density curve appear in the ratios a_1 / a_2 (5). The accuracy of the calculated line ratios is most likely better than 20 % in all cases. Since, however, the long-wave part of the calibration curve was obtained in several successive steps, a systematic error could be propagated. From eq. (5) one gets

$$\left|\frac{\Delta V}{V}\right| = \left|\frac{\Delta R}{R}\right| + \left|x \cdot (\ln 10) \cdot \frac{\Delta x}{x}\right| \qquad (18)$$

With $V \equiv a_1 / a_2$ and $x \equiv D_1/_1 - D_2/_2$

That is, the error due to the relative indaccuracy of x is itself a function of x and becomes smaller with x. It therefore depends on the individual case and cannot be generalized. The inaccuracy in the density measurement can be neglected relative to the error in γ ($\Delta\gamma/\gamma \approx 0.2$). According to eq.(18) an inexactly measured γ value can make the error $\Delta V/V$ much larger than 20 % if only x is large enough. This error, however, is partly eradicated again in determining unknown line intensities, provided that the unknown intensity does not differ too much from that of the calibration line in its vicinity.

As Fig.4 shows, the calibration curve is confirmed in the long-wave part within 20 % by the line ratios of the lithium-like ions; furthermore, in the short-wave region, which is connected with the long-wave part by branching ratios, the curve agrees well with the prediction. It can be assumed from this fact and the errors discussed above that the error in the long-wave region most likely remains below 50 % and does not exceed 100 % in the short-wave part. This assumption is based on a maximum possible error; Fig. 4 shows that no calibration point deviates from the centre part of the curve by more than 40 %.

3.4 Absolute calibration of the spectrograph

In order to link the relative calibration with absolute intensity values, the following approach is usually adopted /24/: The energy input from a line into the spectrograph integrated over time is measured and the plate density achieved is assigned to this energy. The total energy emitted by the plasma in the line is found by determining the fraction of the total energy reaching the entrance slit because of the geometrical conditions. This measurement involves a good deal of uncertainty. In this experiment it is primarily the radiation losses that are of interest, not the energy actually entering the slit. Absolute calibration was therefore done in such a way that the plate density could be assigned direct to the total energy emitted. The procedure is described in the following.

If the emission coefficient of a line $\epsilon(\Omega, \vec{r}, t)$ is known and radiation absorption in the plasma can be neglected, the total energy E_L emitted by this line is obtained by integrating over

the solid angle Ω , the volume V, and the radiation time t:

$$E_L = \int_{\Omega} \int_{V} \int_{t} \epsilon\,(\Omega, \vec{r}, t)\, d\Omega\, dV\, dt \qquad (19)$$

A fraction E of this energy E_L reaches the spectrograph and produces a certain plate density:

$$D = \gamma \log(SE) \qquad (1) \text{ see Section 3.2}$$

with $$E/E_L \equiv G \qquad (2o)$$

eq.(1) yields

$$D = \gamma \log\,(sGE_L). \qquad (21)$$

The goemetrical factor G is constant for all lines investigated if it can be assumed that the radiation emission is isotropic and the spatial distribution (not the absolute value) of $\epsilon\ (\vec{r})$ is always the same. Thus, if $\epsilon_o\ (\vec{r}, t)$ is known for a calibration line, eqs. (19) and (21) yield G, and this allows the total energy emitted by an unknown line to be determined:

$$E_L = E_{Lo} \cdot 10^{D/\gamma - D_o/\gamma} \cdot \frac{s_o}{s} \qquad (22)$$

Quantities with the subscript "o" refer to the calibration line.

The measurement of the emission coefficient of a calibration line that is required for absolute calibration can be done indirectly by measuring the emission coefficient of a line emitted in the visible that is connected with the grazing incidence calibration line by a branching ratio. This measurement can only be done side-on because Abel inversion of intensity profiles measured end-on is practically impossible. Fig.6 shows the set-up for absolute measurement of ϵ_o. A monochromator absolutely calibrated by comparison with a tungsten ribbon lamp is used to determine the intensity profile of the line emitted in the visible. As the plasma is cylindrically symmetric, the emission coefficient is obtained in the usual way by Abel inversion[1]. Equation (19) applied to this

[1] A computer programme developed by Kaufmann /26/ was used for the purpose.

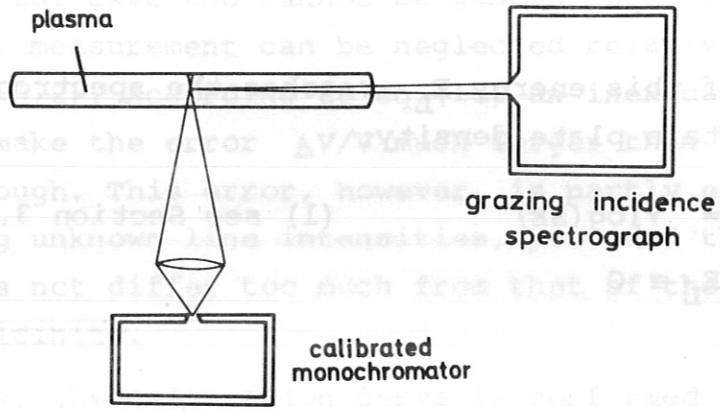

Fig.6: Schematic diagram of the experimental set-up for absolute calibration

geometry yields:

$$E'_{Lo} = \int_0^\infty \left[4\pi \cdot L \cdot \int_0^\infty 2\pi r \cdot \epsilon'_o(r)\, dr \right] dt \qquad (23)$$

where L is the plasma length. Integration over the solid angle Ω yields a factor 4π because it is assumed that ϵ'_o is isotropic. The energy E_{Lo} emitted in the grazing incidence line is then

$$E_{Lo} = R \cdot E'_{Lo} \qquad (24)$$

where R denotes the appropriate branching ratio.

Two branching ratios of the lithium-like ions NV and OVI are used for absolute calibration /25/. The corresponding transitions are listed in Table 3 /12/. While the two doublet components could not be resolved in either of the short-wave lines, this could be readily done in the case of the long-wave lines. The more intense transition $^3S_{1/2} - {}^3P_{3/2}$ was compared with the composed transition 2S - 3P.

Transition	O VI		N V	
	λ (Å)	A ($10^8 sec^{-1}$)	λ (Å)	A ($10^8 sec^{-1}$)
$2S_{1/2} - 3P_{3/2}$	150.088	259	209.270	119
$2S_{1/2} - 3P_{1/2}$	150.124	259	209.303	119
$3S_{1/2} - 3P_{3/2}$	3811.35	0.513	4603.83	0.415
$3S_{1/2} - 3P_{1/2}$	3834.24	0.503	4619.90	0.411
Branching ratio R	1.92×10^4		9.38×10^3	

Table 3: Wavelengths (λ) and transition probabilities (A) of the calibration lines

There must be statistical population of the sub-levels in this case. The correctness of this assumption was checked by comparing the intensities of the two long-wave components. The corresponding branching ratio R (short-to-long-wave transition) is given in Table 3. For reasons of intensity a small percentage (0.5%) of oxygen or nitrogen was added to the filling gas (D_2) for calibrating.

As absolute calibration was done with two pairs of lines of different ions, the already measured sensitivity ratio of the instrument $s(\lambda_1) / s(\lambda_2)$ is again obtained independently for the wavelengths stated in Fig.4. It can be seen that these experimental points are a good fit to the relative variation $s(\lambda)$. The assumption underlying the absolute calibration are thus verified, at least for the ions NV and OVI. These assumptions will now be discussed in somewhat greater detail.

Equation (19) postulates that the absorption be negligible, i.e. that the lines be optically thin. This applies only to beam directions perpendicular to the plasma axis, but not to radiation parallel to the axis, which the spectrograph records end-on. In the next section it is shown how the resulting error can be corrected.

Isotropy of the radiation was again assumed when integrating (23). This is doubtless correct because the ions are not directed in any way (magnetic fields being too weak) and emit independently of one another. The most severe restriction on the correctness of the calibration method is the assumption of equal spatial distrubution of all emission coefficients (22). This, of course, is never strictly satisfied. Even when the impurity density is proportional to the plasma density and the latter has the same profile for all discharge conditions, the density distribution of various stages of ionization of the impurity atoms is not always the same because near the plasma axis the temperatures and densities are higher than in the boundary regions. Ions with low ionization energy thus decay more quickly in the centre than at the boundaries. As regards the ionization energy, the ions emitting the calibration lines should therefore not differ too much from the other ions whose radiation is to be measured. It is true that the OVI ion used for calibration has a lower ionization energy than, say, OVIII. On the other hand, however, its energy is so high ($\approx$ 140 eV) that it can only be produced in the hot region of the plasma in which the more fully ionized ions are present.Near the axis it decays relatively fast, but on integration (23) this region only makes a small contribution to the total losses. The error due to the relatively low OVI density on the axis should thus be kept within the limits prescribed for the accuracy of the relative calibration. The correctness of this assumption is supported by comparing the experimental points obtained for the different ions NV and OVI.

3.5 Considerations concerning the optical thickness of the calibration lines.

Hitherto the absorption of the radiation in the plasma has been neglected. This allowed the intensity ratio of two lines to be set equal to the corresponding emission coefficients (3). The extent to which this is justified is examined in the following.

If allowance is made for absorption, the intensity of a line is given by the radiation transport equation:

$$\frac{dJ(\nu)}{d\tau(\nu)} = J(\nu) + \frac{\varepsilon(\nu)}{\varkappa(\nu)} \qquad (25)$$

with

$$d\tau(\nu) = \varkappa(\nu) . dl \qquad (25a)$$

$\tau(\nu)$ denotes the optical thickness of the plasma at the frequency ν, $\varkappa(\nu)$ the absorption coefficient, and dl is the element of length on a line of sight. Since only the Doppler effect can be responsible for the broadening of the lines investigated in the grazing incidence region, the ratio $S = \varepsilon/\varkappa$ is independent of the frequency /27/ in the region of the line, and one can solve eq. (25).

$$J(\nu) = S \cdot (1 - \exp(-\tau(\nu))) \qquad (26)$$

For a Doppler broadened line $\tau(\nu)$ can be expressed by the optical thickness τ_o in the line centre (ν_o) and the 1/e width $\Delta\nu$ of the line profile:

$$\tau(\nu) = \tau_o \cdot \exp\left(-\left(\frac{\nu - \nu_o}{\Delta\nu}\right)^2\right) \qquad (27)$$

with

$$\tau_o = r_o \lambda (\pi M_i c^2 / 2kT_i)^{1/2} n L f \qquad (27a)$$

r_o = classical electron radius, λ = wavelength of the line

M_i = ion mass
kT_i = ion temperature
} of the impurity ion

n = population of the lower level, L = plasma length
f = absorption oscillator strength of the particular transition.

The total intensity J_L emitted by a line is obtained by integrating eq. (26) over the frequency:

$$J_L = S \cdot \int_{-\infty}^{+\infty} (1 - \exp(-\tau(\nu))) d\nu = S \cdot F(\tau_o) \qquad (28)$$

The function $J_L/S = F(\tau_o)$ is plotted in Fig.7 (curve II). If no allowance is made for absorption, J_L will be proportional to τ_o (curve I). If function I is divided by function II, this provides a measure of the deviation due to neglecting the absorption (curve K). It can be seen that for an optical thickness of $\tau_o = 1$ in the line centre neglecting the absorption causes an error of 40 % in the total line intensity J_L. This is much smaller than the error that would have resulted by just allowing for the intensity in the line centre (curve III). As the calibration error is also of the order of 40 %, it is sufficient merely to postulate $\tau_o < 1$ and not $\tau_o \ll 1$ when measuring the total line intensity in order to satisfy the requirement of optically thin radiation. This follows from the fact that the absorption in the line wings is always smaller than in the centre.

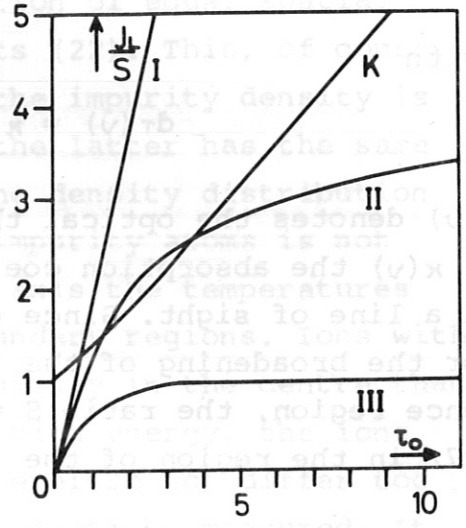

Fig.7: Line intensities as functions of the optical thickness (for explanation see text)

The danger of $\tau_o < 1$ not being satisfied is mainly present for resonance lines. The optical thicknesses for the first Lyman line of CVI and for the transitions 2S-3P of OVI and NV were calculated from eq.(27a). For this purpose a low ion temperature of 200 eV and a high ground state density (0.5% of the electron density) were assumed. This yields an upper estimate. The result is shown in the following table:

Ion	Wavelength (Å)	τ_o
CVI	33.736	3.7
OVI	150.1	12
NV	209.3	15

For a lower estimate of τ_o a rough upper limit of 1 keV is taken for T_i and 0.1 % of the electron density for the mean ground state density. It is shown that the τ_o values are then a factor of 10 lower. The CVI line is thus optically thin. It can be assumed that this also applies in the experiment to the corresponding lines of all hydrogen-like ions because no impurities were added to the filling gas when determining the line intensities in the Lyman series. For the calibration lines of the lithium-like ions, on the other hand, allowance must definitely be made for the optical thickness owing to 0.5 % impurity added. Within the scope of this estimate the intensity of the lines can only be determined exactly to a factor of 5 because of the uncertainty about τ_o. It was therefore attempted to measure the optical thickness direct.

According to eq. (27a) τ_o is proportional to the ground state density and the latter is proportional to the degree of contamination (α), thus τ_o can be increased by raising α. The relation between the relative line intensity and τ_o is given by eq.(28):

$$J_{rel} = A \cdot F(\tau_o) = A \cdot F(B \cdot \alpha) \qquad (29)$$

A and B are proportionality factors. The measured relative intensity values for various degrees of impurity can be fitted to eq. (29) to give A and B. Finally, τ_o is obtained from $\tau_o = B \cdot \alpha$.

α was determined by using the optically thin line 2P - 3S of OVI. The relative intensity of this line was plotted as a function of the added impurity α_z (Fig.8). Extrapolation to the intensity 0 yielded the natural degree of impurity α_o. The actual degree of impurity is the sum of the two components α_o and α_z. Finally, Fig.9 shows the relative intensity of the OVI calibration line plotted as a function of α. Fitting yields B = 9.5 and hence $\tau_o = 5.5$ for an impurity of $\alpha_z = 0.5$ %. This

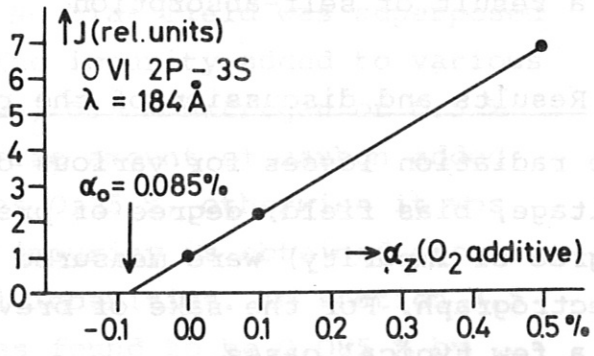

Fig.8: Relative intensity of an OVI line v.oxygen added

τ_o value is within the margins of the above estimate. Fig.7 (curve K) gives a correction factor $K_o = 3.4$ for $\tau_o = 5.5$, i.e. the intensity of the OVI calibration line measured end-on is a factor of 3.4 smaller than would be expected in the optically thin case because of the absorption. This correction has to be allowed for in eq. (22), and the radiation loss of an unknown line is finally given by:

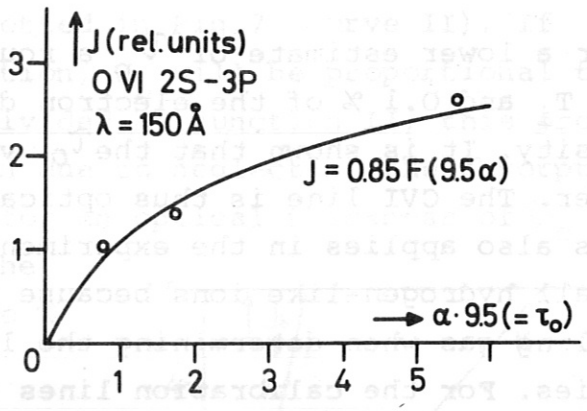

Fig.9: Relative intensity of the OVI calibration line v. degree of oxygen impurity

$$E_L = E_{Lo} \cdot 10^{D/\gamma - D_o/\gamma_o} \cdot \frac{s_o \cdot K}{s \cdot K_o} \qquad (30)$$

For most of the lines investigated K was found to be 1; in exceptional cases it was determined by the method described.

Strictly speaking, eq. (30) with allowance for absorption is no longer right even after correction because it was assumed in eq. (19) that the emitted radiation does not affect the plasma. As the ratio of the longitudinal to the lateral extent of the plasma is approximately 100, by far the greater part of the radiation at end-on τ_o values of less than 10 will be emitted in the optically thin direction, and so there is practically no change in eq. (30) as a result of self-absorption.

4. Results and discussion of the radiation measurements

The radiation losses for various discharge parameters (charging voltage, bias field, degree of preionization, filling pressure, degree of impurity) were measured by means of the calibrated spectrograph. For the sake of brevity, attention is restricted to a few typical cases.

The following questions are of interest:

1) How do the radiation losses depend on the type and degree of impurity?

2) How is the radiation distributed over the individual stages of ionization of one and the same impurity atom?

3) Which transitions of an ion are mainly involved in the radiation losses?

4) How high are the radiation losses relative to the energy content of the electron gas?

The necessary measurements were always made under the same discharge conditions and with a known quantity of added impurity. This afforded comparable and reproducible conditions. No impurities were added for investigating the following questions:

5) How do the radiation losses depend on the initial conditions (filling pressure, bias field), and how high are they under these conditions compared with the energy content of the electrons?

6) How does the radiation power loss depend on the time?

7) How high is the power loss compared with the thermal conduction losses?

Questions 1) to 5) were answered by evaluating time integrated spectra. Questions 6) and 7) were treated by means of time resolved, photoelectric measurements.

4.1 Time integrated measurements

4.1.1 Radiation losses with added impurities

The filling pressure for the measurements in this section was chosen to be 40 mTorr deuterium. No bias field was superposed for reasons of reproducibility. The impurity added to various discharges was either 0.5 % oxygen, 0.5 % nitrogen or 0.5 % methane, relative to the volume. The amount of carbon added relative to the atomic density was 0.25 %, otherwise it was also 0.5 %. The actual degree of impurity is obtained from the sum of the natural and artificial impurities. In section 3.5 the degree of natural impurity was found to be 0.085 % by means of an optically thin OVI line. With 0.5 % additive the radiation losses will thus rise by a factor of 7 if all lines are optically thin and the plasma parameters are not changed by

the additive. This increase is in fact measured. Conversely, the degree of natural impurity can be determined by comparing the radiation losses in discharges with and without additive. This was done for nitrogen and carbon. Unfortunately, the natural carbon impurity, which is caused by creepage of the diffusion pump oil on the vessel wall, is not very reproducible, and so the true degree of impurity cannot be determined exactly. Because of the linear dependence of the radiation losses on the degree of impurity the losses can be related to a uniform degree of impurity. They were normalized for 1 %, the results being given in Table 4. The degree of impurity actually present is given each time.

	Oxygen	Nitrogen	Carbon
Additive + degree of natural impurity	0.5 + 0.085 %	0.5 + 0.0025 %	0.25 + 0096 %
Radiation energy of individual ions	OVI 4.4 OVII 14.1 OVIII 2.6	NV 0.95 NVI 5.1 NVII 8.0	CV 2.8 CVI 24.9

Table 4: Total radiation losses (in joules) for various impurities, normalized for 1 % impurity

The energies for carbon are not only inexact for the reasons already stated: It can be seen from Fig.4 that the sensitivity of the instrument for the resonance lines CV 40.27 Å and CVI 33.74 Å is comparatively high. This results in high densities and hence appreciable decreases in the accuracy of the intensity determination according to Section 3.3.4. An error of 100 % has therefore to be accepted. Apart from this inaccuracy, it can be seen that the total losses for each of the three types of impurity are of about the same order of magnitude. No distinct dependence on the atomic number can be deduced. The energies on the other hand, are distributed in characteristic manner over the successive stages of ionization of one and the same atom: The lighter the atom the more weight is there on the highest hydrogen-like stage.

Comparison of the emitted energy with the total energy content of the electrons show that the radiation losses for 1 % impurity represent only a small fraction. For an electron temperature of 200 eV, filling pressure of 40 mTorr and a vessel volume of 6.35×10^3 cm^3 the energy content of the electrons is about 500 joules; only about 4 % of this energy is emitted. It is therefore not expected that the electron temperature will be greatly influenced by emission in the case of impurities of less than 5 %. Under these conditions it can then be expected that the losses grow in proportion to the degree of impurity, as was established above. Between 5 and 10 % impurity the emission becomes noticeable compared with the electron energy, the electrons are cooled, and so the growth of the losses is less than linear. This applies, of course, only to the plasma parameters for 40 mTorr (see Fig.1).

In order to assess the total radiation losses, it is best to consider the distribution of the emitted energy at the transitions within one stage of ionization. Calculation of the intensity rations of lines of hydrogen-like ions (Section 3.3.1) already showed that more than 90 % of the energy is emitted by the 1S - 2P resonance transition. The same result is obtained in the measurements for the helium-like ions when the forbidden intercombination transition is included. In the case of the lithium-like ions the 2S - 3P and 2P - 3D transitions emit more than 90 % of the energy of all lines in the grazing incidence region. The 2S - 2P resonance transition is outside this region and can, it is estimated, again emit energy of the same order of magnitude as the grazing incidence lines. Since, however, the contribution of, for example, the OVI intensity is small compared with the higher stages of ionization (Table 4), the 2S - 2P transition can be neglected as regards the total radiation losses.

For these reasons only the above listed transitions in the grazing incidence region are taken into account when measuring the total radiation losses in the following.

Filling pressure (mTorr)	Bias field anti-parallel (G)	Losses (in Joules) by Oxygen	Nitrogen	Carbon	Total losses absolute (joules)	with ref. to electron energy (%)	Distribution over ionization stages OVI:OVII:OVIII	NVI:NVII	CV:CVI
11	0	1.33	---	0.14	1.47	0.8	2 : 1 : 0.06	---	1 : 5
	500	18.9	0.017	0.035	19.0	8.0	0.2 : 1 : 0.4	1 : 2	1 : 8
17	0	5.04	0.012	1.34	6.4	2.4	0.8 : 1 : 0.03	1 : 2	1 : 19
	500	54.6	0.024	0.151	54.8	15	0.5 : 1 : 2	1 : 3	1 : 7
40	0	1.76	0.046	2.4	4.22	0.75	0.4 : 1 : 0.2	1 : 2	1 : 24
	500	14.2	0.025	0.73	15.0	2.7	0.3 : 1 : 3	1 : 5	1 : 25
72	0	0.98	0.056	2.35	3.4	0.4	0.3 : 1 : 0.1	1 : 2	1 : 64
	500	2.8	0.097	0.64	3.53	0.4	0.2 : 1 : 0.5	1 : 9	1 : 34

Tabelle 5 Radiation losses in discharges without added impurity

4.1.2 Radiation losses in discharges without added impurity

For the radiation measurements in this section the filling pressure was varied between 10 and 80 mTorr. In some of the discharges an antiparallel magnetic field of 500 G was superposed in order to increase the heating rate and hence the temperature.

The measured total losses and their distribution over the individual stages of ionization are listed in Table 5. The degree of impurity actually present is only known for 40 mTorr and a bias field of 0 G (see Table 4). Measurements of random samples show that in all other cases it is probably between 0.1 and 0.5 %. The big differences in the total losses for various initial conditions are primarily due to various degrees of impurity. This becomes clear in discharges with superposed bias field. In such cases the plasma is contaminated in an irreproducible manner by contact with the wall, the absolute value and also the fluctuations being particularly large. In almost all cases the energy is mainly emitted by oxygen. The emission of the nitrogen ions can practically always be neglected.

It is readily seen that there are big differences in the distribution of the emitted energy over the various stages of ionization. This problem will be discussed in some more detail by taking oxygen as an example. It will be shown that the distribution depends not only on density and temperature but also on the lifetime of the plasma, since we are not dealing with the steady state.

We consider the intensity of the resonance lines of OVII (subscript 1) and OVIII)subsript 2):

$$J_1 = \int \frac{h\nu_1}{4\pi} \cdot n_1' \cdot A_1 \cdot dl$$
$$J_2 = \int \frac{h\nu_2}{4\pi} \cdot n_2' \cdot A_2 \cdot dl \qquad (31)$$

n' = population of the 2P level.

If it is assumed that the absorption is negligible and n' is calculated by means of the excitation coefficients according to Allen /13/ on the assumption of corona equilibrium, the intensity ratio is

$$\frac{J_2}{J_1} = 0.6 \cdot \exp(-81/kT_e) \cdot \frac{n_2}{n_1} \qquad (32)$$

Here n denotes the ground state density, kT_e is measured in eV. If it is assumed that the temperature and density are constant in time and space, and that at the time t = 0 all the oxygen is in the form OVII with the density n_o, the ratio of the total energies emitted after a certain time t is

$$\frac{E_2}{E_1} = 0.6 \exp(-81/kT_e) \cdot \frac{\int_0^t n_2(t')\,dt'}{\int_0^t n_1(t')\,dt'} \qquad (33)$$

with $$dn_1 / dt = - n_1 n_e X + n_2 n_e R \qquad (34)$$

and $$n_1 + n_2 = n_o. \qquad (34a)$$

Here X and R are ionization and recombination coefficients respectively. Further ionization of OVIII is not taken into account. From eqs. (33) and (34) it follows that

$$\frac{E_2}{E_1} = 0.6 \exp(-81/kT_e) \cdot \frac{bt - (1 - \exp(-bt))}{(R/X)\cdot bt + (1 - \exp(-bt))} \qquad (35)$$

$$b = n_e \cdot (X+R) \qquad (35a)$$

Two limiting cases can be distinguished:

For $bt \gg 1$ it follows that

$$E_2 / E_1 \approx 0.6 \exp(-81/kT_e) \cdot (X/R) \qquad (36)$$

for $bt \ll 1$ it follows that

$$E_2 / E_1 \approx 0.6 \exp(-81/kT_e) \cdot \frac{X}{2(R + X)} \cdot bt \qquad (37)$$

Whether one of these limiting cases and which of them is present has to be determined by measuring the plasma parameters and the plasma lifetime. b contains not only the electron density but also the temperature via X and R, which are known in reasonable approximation /28,7/:

$$X = 7.85\cdot 10^{-9} \frac{(kT_e)^{1/2}}{739 + kT_e} \exp(-739/kT_e)\ cm^3 sec^{-1} \qquad (38a)$$

$$R = \frac{1.41 \times 10^{-11}}{(kT_e)^{1/2}} \quad cm^3\ sec^{-1} \qquad (38b)$$

For a temperature of 200 eV and a density of $2 \times 10^{16} cm^{-3}$ eqs. (35a), (38a), and (38b) yield $b = 8 \times 10^4\ sec^{-1}$. High density and temperature can only be maintained experimentally for about 3 - 4 µsec since the plasma is then lost owing to both end losses and strong decrease of the magnetic field. One then gets $bt \approx 0.3$. The limiting case $bt \gg 1$ is obviously not present, the plasma lifetime for the given parameters being too short for a steady state to be achieved. The case $bt \ll 1$ is approximately satisfied. From eq. (37) it is seen that here the energy ratio E_2 / E_1 grows in proportion to the product bt. This result accounts for the pronounced differences in the energy distribution over the individual stages of ionization in Table 5 because under different discharge conditions there are fluctuations in density and temperature, and hence in bt. It can also be seen that it would

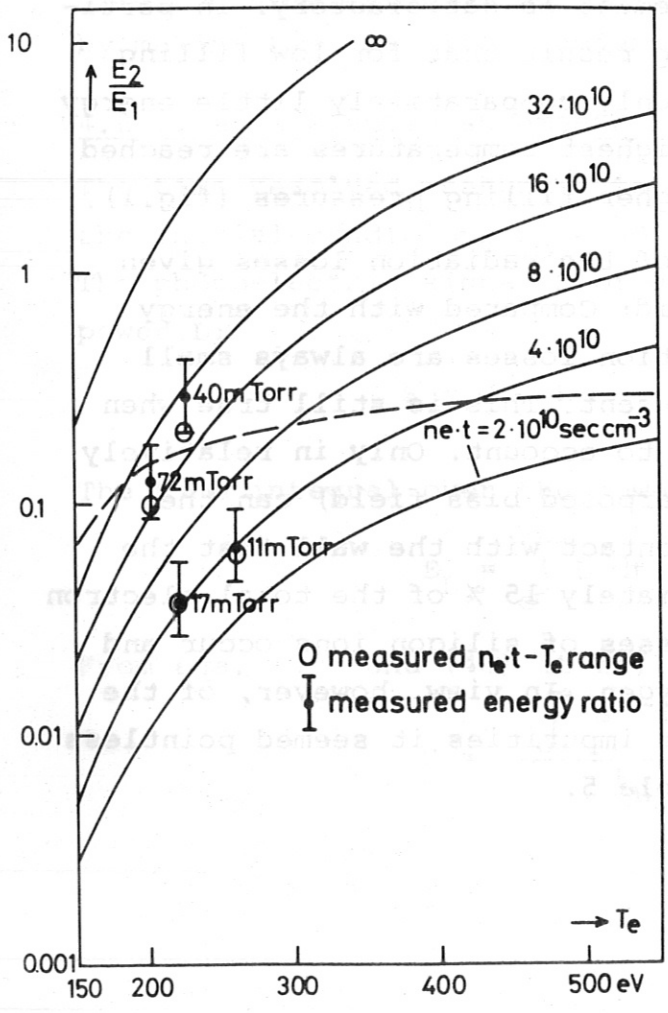

Fig.10

Ratio of energies emitted by the resonance lines OVIII and OVII as a function of electron temperature, electron density, and plasma lifetime.

be pointless to give the measured radiation losses as a function of density and temperature because the steady state is not attained in the short-life plasma concerned, and so the existence of the highly charged ions and hence the absolute value of the radiation losses depends essentially on the lifetime of the plasma. Fig.10 shows the ratio E_2 / E_1 as a function of the temperature and the product $n_e t$ (as parameter).

The experimental values refer to discharges with no bias field superposed.

The dashed curve refers to the case $bt = 1$ ($n_e t = 1/(X + R)$).

It can be seen that slight temperature changes, particularly in the low temperature region, are sufficient to cause pronounced displacement of the ratio E_2 / E_1. The measured intensity ratios can, of course, only be compared with the highly simplified calculation with certain reservations. They have nevertheless been included in the diagram along with the measured range of density, lifetime and temperature. The agreement is satisfactory. In particular, this explains the surprising result that for low filling pressures and a bias field of 0 G only comparatively little energy is emitted by OVIII although the highest temperatures are reached in these cases as compared with higher filling pressures (fig.1).

With regard to the absolute value of the radiation losses given in Table 5 the following can be said: Compared with the energy content of the electrons the radiation losses are always small for the low degrees of impurity present. This is still true when the calibration errors are taken into account. Only in relatively unstable discharges (e.g. with superposed bias field) can the plasma become so contaminated by contact with the wall that the radiation losses amount to approximately 15 % of the total electron energy. In this case additional losses of silicon ions occur and may attain the order of that of oxygen. In view, however, of the complete irreproducibility of these impurities it seemed pointless including the silicon losses in Table 5.

Not taken into account either were the radiation losses due to continuum radiation. An estimate shows that they can be neglected relative to the measured line radiation. If we take $5 \times 10^{16} cm^{-3}$ for the electron density, 300 eV for the temperature, and 1 % OVIII for the degree of impurity, the energy loss due to free-free radiation for a plasma of lifetime of 4 µsec is about 2 joules. This value represents an upper estimate. From Table 5 it can be seen that the line losses are larger; only at 11 mTorr and 0 G are they somewhat smaller than 2 joules, but in this case the density is at least five times as small as assumed above, and so the continuum losses are at most 0.1 joule.

The foregoing has demonstrated that for the degrees of natural impurity present the radiation losses can be discounted as an effective cooling mechanism that limits the electron temperature. It is still conceivable that in certain phases of the discharge, when other mechanisms are not yet effective, the radiation losses exert a dominant influence, but do not essentially affect the electron temperature finally attained. This can only be investigated by making time resolved radiation loss measurements.

4.2 Time resolved measurements

The time resolved measurements are represented by an example with the initial conditions p_o = 40 mTorr, B_o = 0 G, no impurity added. The photoelectric signal S of a line is proportional to the emitted power L:

$$S = C \cdot L \tag{39}$$

The time integral over the power is equal to the emitted energy:

$$E_L = \int_0^\infty L \, dt \tag{40}$$

From eqs. (39) and (40) it follows that

$$C = \frac{\int_0^\infty S \, dt}{E_L} \tag{41}$$

The energies E_L are taken from a plate spectrum. The signals S are obtained from other discharges using the same initial conditions, so that the time behaviour of the radiation power L(t) is always the same. With eq. (41) the calibration factor C is obtained from E_L and S, and with eq. (39) the radiation power L can be given. Its absolute value applies to the conditions under which the plate spectrum was made, even if the degree of impurity for the discharges in which the relative behaviour S(t) was determined should have changed.

Fig. 11 shows the time behaviour of the radiation power loss for the most important ions. It is readily seen that the radiation power of OVI in the initial phase, at about 1 µsec, is larger than that of the more highly ionized ion OVII although more energy is emitted altogether by OVII than by OVI (Table 5). This is due to the shorter lifetime of OVI. This shows that the low ionization stages simply should not be neglected when setting up

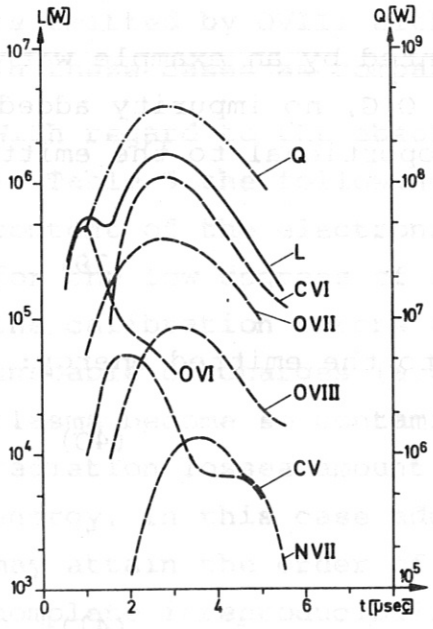

Fig.11
Total radiation losses L and thermal conduction losses Q as functior of time.
Discharge conditions:
p_o = 40 mTorr, B_o = 0 G
Degree of impurity:
0.085 % oxygen
0.096 % carbon
0.0025 % nitrogen

an energy balance, the heating and loss rates being taken into account at every time of the discharge.

The measured radiation power losses are now compared with the thermal conduction losses. The thermal conduction losses are estimated as follows on the lines of Green et al./1/: The plasma is replaced by a homogenious rod of length z_o that is supplied with the energy W per unit length and time. The electron temperature at the ends of the rod is T = O ^{o}K. The thermal conduction equation

$$c\,\varrho\,\frac{\partial T}{\partial t} = \frac{\partial}{\partial z}\left[\,k(T)\,\frac{\partial T}{\partial z}\right] + W \qquad (42)$$

is valid, where c is the thermal capacity, ϱ the density, and k(T) the thermal conductivity.

The boundary conditions are: T = O for z = O
T = O for z = z_o (42a)

The thermal flux Q from the ends of the plasma is

$$Q = 2\,k(T)\,\frac{\partial T}{\partial z}\,.\,F, \qquad (43)$$

taken at the point z = O. F is the cross section of the plasma column. If it is assumed that the stationary temperature profile comes about very quickly compared with changes of W, $\partial T/\partial t$ = O can be substituted in eq. (42) to yield the temperature profile

$$T = T_o\left[\,4\,\frac{z}{z_o}\,(1 - \frac{z}{z_o})\,\right]^{2/7} \qquad (44)$$

with

$$T_o = \left(\frac{7\,z_o^2\,W}{16\,\beta}\right)^{2/7} \qquad (44a)$$

This involves using Spitzer's thermal conductivity /29/:

$$k = \beta\,.\,T^{5/2} \qquad (45)$$

The finally yields Q:

$$Q = \frac{16}{7}\,\beta\,\frac{T_o^{7/2}}{z_o}\,.\,F \qquad (46)$$

As various assumptions on the heating and loss mechanisms are made in estimating W, Q was determined direct from the measured temperatures T_o in the midplane of the plasma. The result appears in Fig.11. The errors of Q are governed primarily by the experimental errors of the temperature determination, by the inaccuracy of F, and by the assumption $\partial T/\partial t = 0$. The temperature was measured with an accuracy of 15 % by means of the Thomson scattering of laser light. The plasma cross section F can be determined within 50 % from the electron density profiles. The deviations of the stationary temperature profile (44) from that actually present cause an error of about 30 % in Q. This emerges from a comparison of the estimated Q values with numerical results of Schneider /30/. It would thus seem that, on the whole, the estimate is correct to a factor of 2 - 3. Even if allowance is made for this element of uncertainty, the thermal conduction losses in the case of natural contamination are two orders of magnitude as high as the radiation losses at practically every time of the discharge, as Fig. 11 shows. Only when the degree of oxygen impurity is increased by a factor of 50 (= 4.5 % additive) can the radiation losses of OVI perhaps predominate in the early phase of the discharge, especially since the OVI losses are in fact even higher owing to the neglected 2S - 2P transition. The decrease of the electron temperature observed /31/ in the initial phase of the discharge by adding 2 % oxygen is thus confirmed.

5. Conclusions

The essential results of this investigation are now summarized. Hitherto only rough theoretical estimates have been available on the radiation losses of a theta pinch plasma. Here these losses are determined experimentally. The radiation of such a plasma ($n_e = 1 - 5 \times 10^{16}$ cm^{-3}, $T_e = 150 - 350$ eV) is mainly emitted at wavelengths between 10 and 200 Å by lines of light impurity ions (e.g. oxygen). Although this region is accessible with a grazing incidence spectrograph, for such short wavelengths there is no radiation standard with which to calibrate the instrument.

Using calculable intensity ratios of lines and applying the branching ratio method it was possible first to calibrate the spectrograph relatively and then to assign it to a radiation standard in the visible. This allowed the radiation losses to be measured

absolutely, both integrated and resolved in time.

The investigations were made over wide density and temperature ranges. It was found that the radiation losses are negligible compared with both the energy content of the electrons and the thermal conduction losses. This applies for the small degrees of impurity present in the deuterium plasma of about 0.1 - 0.5 % foreign atoms. For impurities of the order of 5 %, however, the radiation losses gain in influence and may exceed the thermal conduction losses in early phases of the discharge. Yet even then the electron temperature finally attained is not essentially affected.

Acknowledgments

The author wishes to thank Professor E. Fünfer for the opportunity of conducting these experiments in his division of the Institut für Plasmaphysik.

He is indebted to Professor H. Zwicker for his keen interest in the progress of the investigations.

Dr. W. Köppendörfer is thanked for many useful suggestions and discussions.

Appreciation is also due to many colleagues of Exp. Division 1 who contributed to the success of this investigation.

References:

/1/ T.S.Green, D.L.Fisher, A.H.Gabriel, F.J.Morgan, A.A.Newton, Phys.Fluids 10 (1967) 1663

/2/ R.F.Post, Plasma Physics 3 (1961) 273

/3/ Alan C.Kolb, R.W.P.McWhirter, Phys.Fluids 7 (1964) 519

/4/ D.Düchs, H.R.Griem, Phys.Fluids 9 (1966) 1099

/5/ D.P.Cox, W.H.Tucker, Astrophys.J. 157 (1969) 1157

/6/ R.L.Kelly, NRL Report 6648 (1968)

/7/ R.W.P.McWhirter, in "Plasma Diagnostic Techniques", Academic Press, New York 1965

/8/ G.Klement, A.Knobloch, R.C.Kunze, G.Nützel, H.Schlageter, Laboratory Report IPP 4/58 (1968)

/9/ W.Köppendörfer et al., Laboratory Report to be published

/10/ R.Lincke, in "Plasma Diagnostics", North-Holland Publishing Company, Amsterdam 1968

/11/ P.Bogen, in "Plasma Diagnostics", North-Holland Publishing Company, Amsterdam 1968

/12/ W.L.Wiese, M.W.Smith, B.M.Glennon, "Atomic Transition Probabilities", Vol.I, NSDS - NBS 4 (1966)

/13/ C.W.Allen, "Astrophysical Quantities", 2nd Edition, The Athlone Press, London 1963

/14/ J.D.Garcia, J.E.Mack, JOSA 55 (1965) 654

/15/ H.R.Griem, "Plasma Spectroscopy", McGraw-Hill Book Company, New York 1964

/16/ B.L.Moiseiwitsch, S.J.Smith, Rev.Mod.Phys.40 (1968) 238

/17/ L.A.Vainshtein, Opt.Spectry. USSR 18 (1965) 538

/18/ I.C.Percival, M.J.Seaton, Phil.Trans.Roy.Soc.London 251A (1958) 113

/19/ W.L.Wiese, A.W.Weiss, Phys.Rev. 175 (1968) 50

/20/ W.L.Wiese, private communication

/21/ C.Mahn, Zeitschr.f.Naturforschung, 22a (1967) 1939

/22/ O.Bely, Proc.Phys.Soc.London 88 (1966) 587

/23/ A.P.Lukirskii, E.P.Savinov, O.A.Ershov, Yu.F.Shepelev, Opt.Spectry. 16 (1964) 168

/24/ F.J.Morgan, A.H.Gabriel, M.J.Barton, J.Sci.Instr.1(1968) 998

/25/ H.J.Kunze, W.D.Johnston, 9.Int.Conf.Phen. Ion.Gases, Bukarest 1969

/26/ M.Kaufmann, private communication

/27/ W.W.Köppendörfer, R.C.Elton, 8.Int.Conf.Phen.Ion.Gases, Wien 1967

/28/ H.-J.Kunze, A.H.Gabriel, Hans R.Griem, Phys.Rev. 165 (1968) 267

/29/ L.Spitzer jr., "Physics of Fully Ionized Gases", 2nd Edition, Interscience Publishers, New York 1967

/30/ W.Schneider, private communication

/31/ A.D.Beach, H.A.B.Bodin, C.A.Bunting, D.J.Dancy, G.C.H.Heywood, M.R.Kenwood, J.McCartan, A.A.Newton, I.K.Pasco, R.Peacock, J.L.Watson, Culham-Report CLM-P 198 (1969)